

# VAE-LoCo: Versatile Quadruped Locomotion by Learning a Disentangled Gait Representation

Alexander L. Mitchell<sup>✉</sup> Wolfgang Merkt<sup>✉</sup> Mathieu Geisert<sup>✉</sup> Siddhant Gangapurwala<sup>✉</sup>  
 Martin Engelcke<sup>✉</sup> Oiwi Parker Jones<sup>✉</sup> Ioannis Havoutis<sup>✉</sup> Ingmar Posner<sup>✉</sup>

**Abstract**—Quadruped locomotion is rapidly maturing to a degree where robots now routinely traverse a variety of unstructured terrains. However, while gaits can be varied typically by selecting from a range of pre-computed styles, current planners are unable to vary key gait parameters *continuously* while the robot is in motion. The synthesis, on-the-fly, of gaits with unexpected operational characteristics or even the blending of dynamic manoeuvres lies beyond the capabilities of the current state-of-the-art. In this work we address this limitation by learning a latent space capturing the key stance phases constituting a particular gait. This is achieved via a generative model trained on a single trot style, which encourages disentanglement such that application of a *drive signal* to a single dimension of the latent state induces holistic plans synthesising a continuous variety of trot styles. We demonstrate that specific properties of the drive signal map directly to gait parameters such as cadence, footstep height and full stance duration. Due to the nature of our approach these synthesised gaits are continuously variable online during robot operation and robustly capture a richness of movement significantly exceeding the relatively narrow behaviour seen during training. In addition, the use of a generative model facilitates the detection and mitigation of disturbances to provide a versatile and robust planning framework. We evaluate our approach on two versions of the real ANYmal quadruped robots and demonstrate that our method achieves a continuous blend of dynamic trot styles whilst being robust and reactive to external perturbations.

## I. INTRODUCTION

Quadruped locomotion has advanced significantly in recent years, extending their capability towards applications of significant value to industry and the public domain. Driven primarily by advances in optimisation-based [1]–[4] and reinforcement learning-based methods [5]–[7], quadrupeds are now able to robustly plan traversals over a wide variety of terrains, which makes them an increasingly popular choice for tasks such as inspection, monitoring, search and rescue or goods delivery in

This work was supported by a UKRI/EPSC Programme Grant [EP/V000748/1], the EPSRC grant ‘Robust Legged Locomotion’ [EP/S002383/1], the EPSRC CDT [EP/L015897/1], the UKRI/EPSC RAIN [EP/R026084/1] and ORCA [EP/R026173/1] Hubs and the EU H2020 Project MEMMO (780684). It was conducted as part of ANYmal Research, a community to advance legged robotics. (*Corresponding author: Alexander L. Mitchell.*)

Alexander L. Mitchell, Wolfgang Merkt, Siddhant Gangapurwala, Oiwi Parker Jones, Ioannis Havoutis, and Ingmar Posner are with the Oxford Robotics Institute, Department of Engineering Science, University of Oxford, U.K. (e-mail: mitch@robots.ox.ac.uk; wolfgang@robots.ox.ac.uk; siddhant@robots.ox.ac.uk; oiwi@robots.ox.ac.uk, ioannis@robots.ox.ac.uk, ingmar@robots.ox.ac.uk).

Mathieu Geisert is with Arrival Ltd., London, U.K. Work done while at Oxford.

Martin Engelcke is with DeepMind Technologies Ltd., London, U.K. Work done while at Oxford.

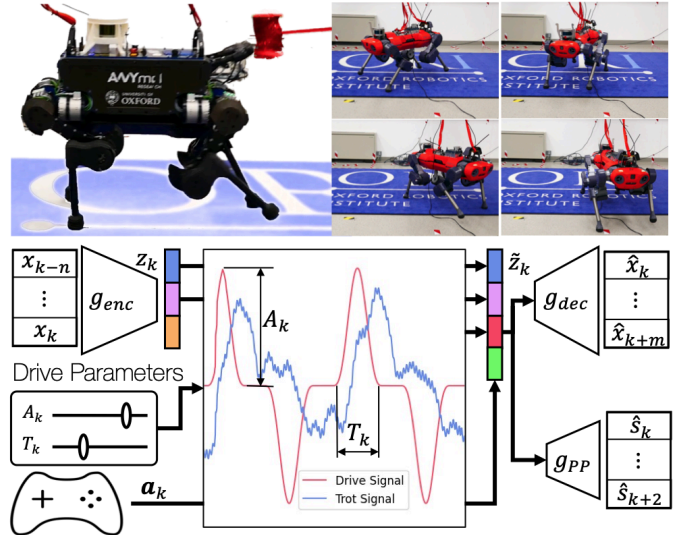


Fig. 1: Using a variational auto-encoder (VAE), our approach learns a structured latent space capturing key stance phases constituting a particular gait. The space is disentangled to a degree such that application of a *drive signal* to a single dimension of the latent variable induces gait styles which can be seamlessly interpolated between. The drive signal’s amplitude and phase provide continuous control over the gait parameters such as cadence, full-support duration and foot swing height. Meanwhile, the amplitude of the inferred *trot signal* governs footstep distance given the user-controlled base twist  $\mathbf{a}_t$ . We encode raw sensor information to infer the robot’s gait phase using  $g_{enc}$  and append an action vector, which expresses the desired base twist, to the augmented latent variable before decoding via  $g_{dec}$ , and predicting the feet in contact using  $g_{pp}$ . This approach readily transfers from ANYmal B to ANYmal C, a dynamically dissimilar robot, without retraining. Additionally, we measure disturbances as out of distribution seen during training and adjust cadence as a rudimentary, but effective response.

difficult, unstructured environments. However, despite recent advances, important limitations remain. Due to the complexity of the system, models used for gait planning and control are often overly simplified and handcrafted for particular gait types (e.g. crawl, trot, gallop, e.g. [1], [8]). In the worst case, this can limit the versatility of the robot as the models deployed are failing to exploit the full capability of the underlying hardware (e.g. [1], [9], [10]). Furthermore, current gait planners are unable to vary key parameters (such as step height) of a gait

continuously and online [3], [4]. Instead, contact schedules for discrete gaits are often pre-computed and selected as needed using hierarchical approaches that rely upon a sequence of optimisations, yielding only a narrow operating window which severely limits their response to external disturbances [3], [4]. The synthesis of gaits which fall outside of this set is typically cumbersome, as approaches that optimise dynamics over gait schedules and footstep lengths or heights are computationally expensive [3], [4], and often require manual intervention [1]. In contrast, the ability to control key gait parameters – such as cadence, swing height, and full-support duration – *on-the-fly* would enable a smooth interpolation between dynamic manoeuvres allowing for swift reaction to external stimuli. This leads to significantly more versatile locomotion.

Inspired by recent work on a quadruped that achieves a crawl gait via the traversal of a learned latent space [11], we approach the challenge of continuous contact schedule variation from the perspective of learning and traversing a structured latent-space. This is enabled by learning a *generative model* of locomotion data which, in addition to capturing relevant structure in the latent space, also enables the detection and mitigation of disturbances to provide a versatile and robust planning framework. In particular, we train a variational auto-encoder (VAE) [12], [13] on short sequences of state-space trajectories taken from a single gait type (trot), and predict a set of future states. We show that the resulting latent space has an interpretable structure, lending itself to the generation of a variety of trot styles, depending on how the latent space is traversed. In fact, examining trot trajectories in latent space reveals an oscillatory drive signal which controls fundamental aspects of the gait. We subsequently find that by overwriting this trajectory with a synthetic drive signal, we can *continuously* control the robot’s gait properties whilst the robot is executing the motion. Parameters of this drive signal can be mapped explicitly to gait parameters such as cadence, footstep height, and full-stance support duration. We emphasise that this ability to generalise over gait styles emerges from training on a single gait type: a trot gait with constant parameters.

We illustrate the efficacy of our approach by generating a range of continuously blended trajectories firstly on the real ANYmal B quadruped robot – a medium-sized platform (35 kg) standing 0.5 m tall. Subsequently with no retraining, we repeat the experiment on the heavier ANYmal C quadruped, which weighs in at 50 kg and delivers twice the peak torque of the former platform. This demonstrates not only transfer from simulation to the real robot, but to a dynamically dissimilar platform crucially without retraining. While the latent space is learnt using examples only from a specific gait style, our approach is able to synthesise behaviours significantly beyond this training distribution.

In addition, we leverage our generative approach to both characterise and react to external perturbations. A large impulse applied to the robot’s base triggers a spike in the Evidence Lower Bound (ELBO) which clearly identifies the disturbance as out of the distribution seen during training. Inspired by [14], which states that an increase in cadence is both a response to slip and a form of push recovery in humans, our planner automatically increases the robot’s cadence to aid

in counteracting the disturbance. This demonstrates a marked improvement in robustness.

To the best of our knowledge, our method is the first which allows continuous variation of the robot’s gait characteristics whilst the robot is walking. It provides a versatile and data-driven approach to quadruped locomotion which additionally allows for disturbance detection and recovery.

### A. Statement of Contributions

This paper extends our previous work, *Next Steps* [15], in order to showcase in-depth analysis of the method previously proposed. This includes significant extensions to key sections of *Next Steps* as well as new analysis which includes deployment on a brand new platform with significantly different dynamics: the ANYmal C.

In particular, we have extended the description and justification for the oscillatory drive-signal in Sec. III-A. In addition, we have significantly extended the interpretation of the latent-space structure and explain at length how the trajectory in this space looks (Sec. VI-A). Additionally, we compare the nominal trajectory in latent space to that seen during the disturbance and recovery phase, significantly expanding on the analysis of the disturbance rejection experiments presented in *Next Steps* (Sec. VI-H). We also extend the discussion of the ablation study of the model’s sensitivity to hyper-parameters (Sec. VI-C).

Additionally, in this paper, we introduce new aspects of analysis. Firstly, we compare how backpropagating the binary cross-entropy (BCE) through the VAE’s encoder effects the latent-space structure (Sec. VI-B). Crisp decision boundaries and axis-alignment are key for latent-space planning such that the contact state alters predictably. We also find that backpropagating the BCE encourages disentanglement between the robot’s step length and height, leading to independent control over the robot’s gait parameters. Secondly, we analyse the receptive field of the VAE’s encoder in order to understand which parts of the input are used to infer the robot’s gait phase. The ability to infer the gait phase is crucial for successful closed-loop planning in latent-space. Hence, analysis of this mechanism is justified, and is found in Sec. VI-D. Thirdly, we compare the dynamic feasibility of the trajectories from the VAE-planner to those seen during training, see Sec. VI-F. This analysis shows that VAE-planner’s locomotion trajectories remain dynamically feasible despite the gait parameters differing from those seen during training. Next, we compare the distribution of realisable gait parameters output from VAE-planner to those seen in the dataset, see Sec. VI-G. In essence, we show the broadness of the range of gaits achievable using our approach and compare this to the distribution in the training set. Lastly since we have shown that the approach can transfer from simulation to the real ANYmal B in *Next Steps*, we push this limit to the next level and deploy the VAE-planner on ANYmal C without retraining, (Sec. VI-I). We utilise this experiment to investigate the extent to which the VAE-planner is able to generalise to out of distribution scenarios. In particular, ANYmal C exhibits significantly different dynamics to ANYmal B. These differences are detailed in Sec. VI-I.

Additionally in Sec. VI-I, we compare the observed robot state trajectory distributions from ANYmal B with ANYmal C using our approach.

## II. RELATED WORK

Planning and control for quadruped locomotion have advanced in leaps and bounds in recent years. A seminal work in these areas is *Dynamic Gaits* (DG) [1]. DG enables a quadrupedal robot (ANYmal) to execute a wide variety of dynamic gaits (e.g. trot, pace, lateral walk, jump) with real-time motion planning and control. However, to achieve this impressive range of behaviours, DG provides each gait type with its own contact schedule and utilises an environment-specific footstep planner, ultimately limiting its capability.

Latent space approaches for planning and control learn useful and typically low-dimensional representations that can be used to control complex dynamics, without relying on known system models. Classic examples include *Deep Variational Bayes Filters* (DVBF) [16] and *Embed to Control* (E2C) [17]. DVBF produces dynamically consistent trajectories by traversing continuous paths in latent space whilst E2C learns a linear system model in which control problems can be solved. *Conditional Neural Movement Primitives* (CNMP) [18] is a more recent latent space approach for robotic arms that generalises between a variety of tasks, such as pick-and-place and obstacle avoidance. Other recent works like UPN and PlaNet [19], [20] show impressive capabilities in simulation but are yet to be applied to real-world systems, including floating-base robots.

In the quadruped domain, *First Steps* [11] learns a structured latent space based on feasible robot *configurations* and then defines a set of performance predictors that can be used in an optimisation framework to control the robot. In practice, these performance predictors can be viewed as symbolic inputs (e.g. ‘left front leg up’) but drive the robot in continuous space. However, because *First Steps* is trained on static snapshots of robot configurations, it does not learn from observable dynamics and thus requires more explicit structuring of the latent space than is necessary. Our previously published work *Next Steps* [15] addresses this shortcoming and significantly extends this framework to effective and robust closed-loop planning and control. In this paper, we provide significantly more in-depth study into continuous variation of the gait parameters via planning in a structured latent-space. In doing so, we further justify the utilisation of an oscillatory drive signal, analyse the quality of the VAE’s trajectories, and push the limits of domain transfer through deployment on new robotic platform without retraining.

The *Motion VAE* (MVAE) [21] learns to represent dynamic trajectories in a structured latent space for the locomotion of computer-animated humanoids. This is similar to our emphasis here on learning representations for dynamic trajectories in the context of locomotion. However, moving from simulated to real physical systems, as is required for robotic applications, necessitates tackling additional complexities like latency, hard real-time requirements, and actuator dynamics. In this work, we tackle these challenges and demonstrate that a single gait

style contains sufficient richness to learn a structured latent space that can be exploited to manipulate gait characteristics that generalise beyond the range seen during training. Unlike MVAE, our approach does not train on multiple gait styles, despite succeeding in producing them.

Finally, a study conducted concurrently to our own [22] yields variation between gait types (walk and trot). It utilises a reinforcement learning (RL) approach which employs a phase iterator similar to our drive signal. However, this phase iterator is enforced, whilst our gait dynamics are discovered automatically purely from exposure to trot trajectories with constant parameters.

## III. APPROACH

Our aim is to use unsupervised learning to infer a structured latent-space which facilitates real-time and smooth variation of key gait parameters. We conjecture that structure can emerge from the exposure of a suitable generative model to a gait with predetermined and constant characteristics such as cadence, swing height, and full-support duration. Specifically, we propose that due to this structure, continuous latent trajectories result in robot locomotion, see Fig. 2. By inspecting this structure, we discover a disentangled latent-space where gait parameters are axis-aligned within this space (Sec. VI-A). Periodic trajectories in latent space can then be decoded back to smooth robot locomotion as depicted in Fig. 1. Subsequently, the VAE is deployed as a planner in a real-time control loop.

**VAE Architecture:** We train a VAE [12], [13] to create a structured latent-space using observed dynamic data. The input to the VAE  $\mathbf{X}_k$  at time step  $k$  consists of  $N$  robot states sampled from simulated trot gaits with constant parameters (e.g. cadence and foot-step height). These state-space quantities are values we wish either to control or are required to infer the gait phase. These are joint angles; end-effector positions in the base frame; joint torques; contact forces; the base velocity; and the base pose evolution relative to a control frame, which is updated periodically. These quantities are denoted as  $\mathbf{x}_k = [\mathbf{q}_k, \mathbf{e}\mathbf{e}_k, \boldsymbol{\tau}_k, \boldsymbol{\lambda}_k, \dot{\mathbf{c}}_k, \Delta\mathbf{c}_k]$ , where  $k$  is the time step. Note that velocities and accelerations do not form part of the VAE’s input, but are inferred from the input history. This has dual benefits: first, it yields a lower-dimensional input space; and, second, it prevents sensitivity to fast-changing quantities such as the recorded joint accelerations during inference.

To deploy the VAE-planner in a closed-loop framework, we encode the input history at the control frequency  $f_c$ . However, due to restrictions on the VAE’s size caused by the tight computation bounds required for real-time control, the encoder input  $\mathbf{X}_k$  is constructed using states spaced at a frequency of  $f_{enc}$ :

$$\mathbf{X}_k = [\mathbf{x}_{k-r(N-1)}^\top, \dots, \mathbf{x}_{k-r}^\top, \mathbf{x}_k^\top], \quad (1)$$

where  $r = f_c/f_{enc}$  is the ratio between the control and encoder frequencies. The input  $\mathbf{X}_k$  is created every time step by sampling from an input buffer which stores every robot state  $\mathbf{x}$  from time step  $k$  to  $k - r(N - 1)$  at the control frequency. We provide full details of the setting used in our experiments in Sec. IV-B.

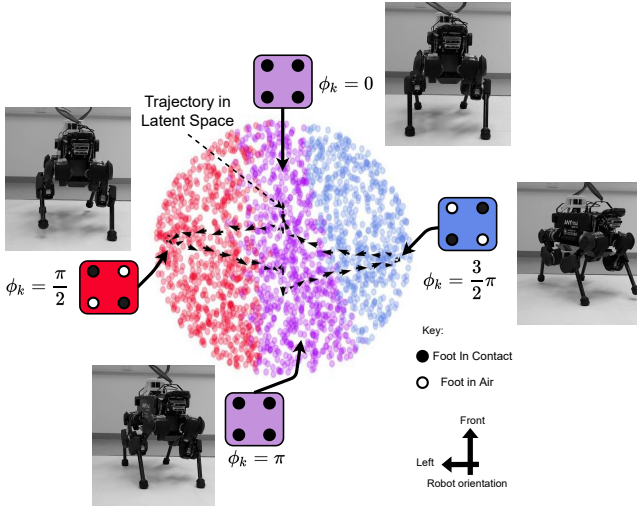


Fig. 2: A slice through the structured latent space, colour coded to illustrate the ordering and clustering of the distinct stances which make up the trot gait. The component of the latent-space trajectory (black) along the horizontal axis contributes to the robot’s footstep height, whilst the vertical component gives rise to the footstep length. Snapshots of the robot controlled using the VAE-planner illustrates the inter-play between these two latent dimensions.

The VAE’s decoder output  $\hat{\mathbf{X}}_k^+$  predicts the current robot state  $\mathbf{x}_k$  as well as  $M$  future ones sampled at a frequency of  $f_{\text{dec}} = f_c$ :

$$\hat{\mathbf{X}}_k^+ = [\hat{\mathbf{x}}_k^\top, \hat{\mathbf{x}}_{k+1}^\top, \dots, \hat{\mathbf{x}}_{k+M}^\top] \quad (2)$$

As the *desired-feet-in-contact* is an input to the tracking controller, we also want to predict which of the four feet are in contact,  $\mathbf{s}_k$ , at the current time step,  $k$ , as well as  $J$  steps in the future. Inspired by *First Steps* [11], we therefore utilise a feet-in-contact performance predictor  $g_{pp}(\mathbf{z}_k)$ . This is attached to the latent space, which estimates the probability of each foot being in contact:

$$\hat{\mathbf{S}}_k = [\hat{\mathbf{s}}_k^\top, \dots, \hat{\mathbf{s}}_{k+J-1}^\top]^\top \quad (3)$$

To command the base twist of the robot, a high-level action command  $\mathbf{a}_k$  is utilised. This represents longitudinal ( $x$ ), lateral ( $y$ ), and yaw ( $\theta$ ) twist in the robot’s base frame. The latent state  $\mathbf{z}_k$  and the action  $\mathbf{a}_k$  form the input to the decoder.

**Training the VAE:** We train the VAE and performance predictor together. The VAE’s training loss is the modified ELBO formulation found in [23]. This loss consists of a reconstruction loss (mean-squared error) plus the Kullback–Leibler (KL) divergence  $D_{\text{KL}}$  between the inferred posterior  $q(\mathbf{z}|\mathbf{X}_k)$  and the prior  $p(\mathbf{z})$ , multiplied by a hyper-parameter  $\beta$ :

$$\mathcal{L}_{\text{ELBO}} = \text{MSE}(\mathbf{X}_k^+, \hat{\mathbf{X}}_k^+) + \beta D_{\text{KL}}[q(\mathbf{z}|\mathbf{X}_k)||p(\mathbf{z})]. \quad (4)$$

These ELBO terms are then summed with the binary cross-entropy loss between the predicted feet in contact and the recorded ones. The latter term is scaled by  $\gamma$ , resulting in the overall loss

$$\mathcal{L} = \mathcal{L}_{\text{ELBO}} + \gamma \text{BCE}(\mathbf{S}_k, \hat{\mathbf{S}}_k) \quad (5)$$

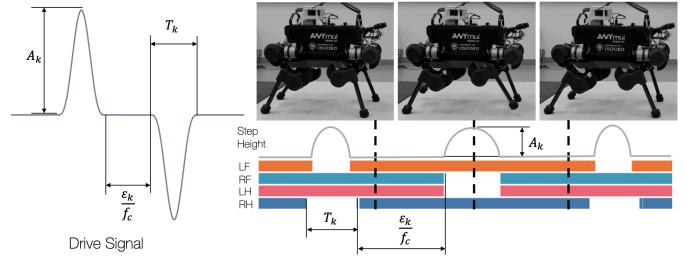


Fig. 3: An oscillatory *drive signal* overwrites the dimension with the smallest variance in the structured latent-space. The amplitude  $A_k$ , time-period  $T_k$  and stance duration counter  $\epsilon_k$  of this signal control the robot’s foot swing height, cadence and full-support duration in real time.

The VAE training loss (Eq. 4), as seen in prior work [23], is responsible for any subsequent disentanglement found in the latent space. The reconstruction error is weighed against the decomposition of the latent space using the hyper-parameter  $\beta$ . This constraint encourages an efficient latent representation, containing only the required information for reconstruction, hence acting to regularise the latent space. As shown in [23], the  $D_{\text{KL}}$  term used with an isotropic unit Gaussian ( $p(\mathbf{z}) = \mathcal{N}(\mathbf{0}, \mathbf{I})$ ) encourages conditional independence within  $\mathbf{z}$ .

In our approach, as well as that of *First Steps* [11], a structured latent space is encouraged by backpropagating gradients from the performance predictor’s loss through to the encoder input. However, we hypothesise that useful structuring of this space is inferred from the continuous trajectories used for training, and, in contrast to *First Steps*, no explicit labelling for each stance is required.

#### A. Control over the gait parameters

Once the VAE has been trained as described above, we discover that the learned latent-space is disentangled. We discover that an oscillation injected into one latent dimension decodes to the robot taking steps. Further analysis detailed in Sec. VI-A finds that adding a second oscillation into the latent space varies the robot’s step length. The former oscillation we denote as the *drive signal*, and the latter as the *trot signal*. We find that in order to control the robot, we only need to inject the drive signal into latent space, and can infer the trot signal. By modulating and visualising the joint-space output from the decoder, we discover that varying the amplitude and phase of the drive signal leads to continuously variable trot locomotion. Therefore, we choose a specific drive signal with features which map directly to the gait parameters we wish to control. These parameters are the robot’s cadence, stance duration and step height.

While any periodic oscillation (e.g. *sin*) decodes to robot locomotion, we choose a drive signal featuring specific components allowing for control over the robot’s cadence, swing duration and step height. The drive signal chosen here is a modified  $\sin^3$  oscillation as depicted in Fig. 3 with amplitude  $A_k$ , and phase  $\phi_k$ :

$$\mathbf{z}_{k,d_z} = A_k \sin^3(\phi_k). \quad (6)$$

The amplitude  $A_k$  controls the foot swing height, and the phase  $\phi_k$  governs cadence and support duration.

To control the robot’s swing and stance duration separately, we set the drive signal’s time-period  $T_k$  and we employ a stance counter  $\epsilon_k$ . The time-period  $T_k$  is equal to the swing duration, whilst the time that the drive signal is equal to zero is extended by  $\epsilon_k$  time steps to introduce a full-support duration of  $(\epsilon_k/f_c)$  s. Hence, once both  $T_k$  and  $\epsilon_k$  are used together, the phase dynamics are:

$$\phi_{k+1} = \begin{cases} \phi_k & \text{if } \phi_k \bmod \pi = 0 \text{ and } k_\epsilon < \epsilon_k \\ \phi_k + 2\pi/T_k & \text{otherwise} \end{cases} \quad (7)$$

and, in tandem, the counter  $\epsilon_k$  is updated as:

$$k_\epsilon \leftarrow \begin{cases} k_\epsilon + 1 & \text{if } \phi_k \bmod \pi = 0 \text{ and } k_\epsilon < \epsilon_k \\ 0 & \text{otherwise} \end{cases} \quad (8)$$

### B. Planning for closed-loop control

Once the VAE is trained, it is fast enough to act as a planner in a closed-loop controller. Thus, our approach can react to external disturbances and mitigate against real-world effects such as unmodelled dynamics and hardware latency. For closed-loop control, we begin by encoding a history of robot states from the raw sensor measurements to infer the current gait phase. We store a buffer of past robot states and sample from this at  $f_{\text{enc}}$  to create the encoder’s input.

With an estimate of the current latent variable, we overwrite latent dimension  $d_z$  with the drive signal (see Sec. III-A). Next, we employ a second-order Butterworth filter to smooth the latent trajectory and further smooth the locomotion plan. In essence, the drive signal encourages the decoder to output the next open-loop prediction while the other latent variables infer the gait phase from the raw sensor input. This process is repeated at the control frequency (400 Hz).

The latent variable  $\mathbf{z}_k$  and a desired base twist  $\mathbf{a}_k$  are decoded to produce  $\hat{\mathbf{X}}_k^+ = g_{\text{dec}}(\mathbf{z}_k, \mathbf{a}_k)$ . From this, the joint-space trajectory  $\hat{\mathbf{Q}}_k$ , and local base velocity  $\hat{\mathbf{C}}_k$  are extracted and derived or integrated to produce the base and joint positions, velocities and accelerations. These quantities and the predicted contact schedule are sent to the whole-body controller (WBC) [24]. The WBC solves a hierarchical optimisation problem to calculate the joint torques which are commands sent to the actuators. The series of constraints enforced by the WBC are: contact creation, friction constraints and torque limits. Next, the WBC applies forward kinematics to the VAE’s trajectory to track it in task-space. Note that the WBC does not compensate for infeasible plans, i.e. the VAE’s trajectories shown in Sec. VI-E are dynamically consistent otherwise the robot fails to walk.

### C. Disturbance detection and response

Our approach is able to both detect and react to disturbances. The VAE is trained using canonical feasible trajectories. Therefore, any disturbances are characterised as out of distribution with respect to the training set. Given the generative nature of our approach, this discrepancy is quantified

during operation by the trained model via the Evidence Lower-Bound (ELBO, Eq. 4 where  $\beta$  is set to one). We will show in the evaluation (Sec. VI-H) that even a rudimentary response strategy serves to increase the range of disturbance the system can reject.

## IV. IMPLEMENTATION DETAILS

In order to deploy the VAE-planner on-board the ANYmal quadruped, there are a number of real-world constraints which affect the VAE-planner. The first of which is that in order to deploy the VAE in a real-time control loop, there is a constraint on the VAE’s inference time. Secondly, we discuss how we address the simulation to reality gap. We discuss the VAE’s specific architecture, the hyper-parameters used to train the model, and finally, specific the specific criteria required for domain transfer.

### A. Dataset generation

To train the VAE and create the structured latent space, we require a set of continuous trot trajectories. In order to study, understand and gain key insight of how to generate versatile locomotion by utilising a structured latent-space, we choose to build a model of locomotion by focusing on flat terrain.

We employ the gait generation framework *Dynamic Gaits* (DG) [1] and solve for trot gaits which track a user-defined base twist command. DG is a hierarchical planning and control framework which is used with a *fixed* contact schedule and predefined footstep heights. Specifically, swing, full-stance durations and footstep height remain constant and are set to 0.5 s, 75 ms and 0.10 m, respectively. This is the only gait style used for training. The main components of DG are a footstep planner, a base motion planner and a whole-body controller (WBC). The footstep planner computes the next four steps over the gait period using an inverted-pendulum model. Using the footstep positions and schedule, the base motion planner computes the base trajectory over the gait period using a centroidal dynamics model [10] constrained with a Zero-Moment Point (ZMP) [9] criterion. The WBC [24] outlined in Sec. III-B then converts the task space trajectories to joint feedforward torques, reference positions and velocities, which are sent to the actuators.

The dataset is generated by uniformly sampling desired base twist and executing DG in the *RaiSim* physics simulator [25]. To improve the fidelity of the simulation, the dynamics of the Series-Elastic Actuators (SEA) [26] in the ANYmal’s joints are modelled using an *actuator network* [5]. This is essential for good performance as the input response of SEAs depends on a history of states, inputs, and the low-level control law. The specific network used here is found in [7], and takes into account the commanded positions, velocities, feed-forward torques, and low-level PD gains.

### B. VAE architecture details

Fig. 1 outlines the approach’s architecture, and here we describe the VAE’s specific details. Prior to the ablation study in Sec. VI-C, the VAE’s encoder, decoder and stance

performance predictor have two hidden layers and widths of 256 units, using ELU non-linearities [27]. The encoder input is created using  $N = 80$  robot states sampled at 200 Hz – representing a history of 0.4 s – from the encoder input, which is of size 5120 units. The input is compressed via a latent space of 125 units which is concatenated with an action of 3 units. Next, the decoder outputs the current state and the next  $M = 19$  robot states at the control frequency of 400 Hz (preview horizon 47.5 ms, output size: 1216 units). The performance predictor predicts the current feet in contact and two future states. Finally, hyper-parameters used for training are  $\beta = 1.0$ ,  $\gamma = 0.5$ , with a learning rate of  $1 \times 10^{-3}$  using the Adam optimiser. Training is terminated after  $1 \times 10^6$  gradient steps.

### C. Domain transfer

To achieve domain transfer and deployment on the real robot, some modifications are required. The contact forces are artificially set to zero when the robot measures no contact (as determined by a probabilistic contact estimator) [28]. This is necessary since the real-world ANYmal robot measures large contact forces even during swing motion, as these forces are inferred from torque residuals and are affected by model error. In contrast, simulators estimate no contact force during swing. As mentioned in Sec. III-B, a Butterworth filter with a cutoff frequency of 10 Hz is employed to smooth the latent trajectory. Due to the strict computation budget for real-time control, inference times for the VAE are restricted to at most 1 ms, which imposes constraints on the capacity of the model (see Sec. VI-C for an ablation of model hyperparameters). Our largest model takes approximately 1 ms for the VAE computation, which is roughly equal to the computation time of the WBC.

## V. EXPERIMENTAL DESIGN

In this section, we explain how the latent-space properties are discovered and how we assess the performance of the VAE-planner deployed on the real robot. In doing so, we motivate the following guiding questions. The aim of these questions is to analyse the latent space once the VAE is trained and to analyse the capabilities of the VAE as a flexible and robust locomotion-planner.

We investigate (i) the structure induced in the latent space (Sec. VI-A), (ii) the effect backpropagating the binary cross-entropy gradients through the encoder has on the latent-space structure (Sec. VI-B) (iii) the sensitivity of our approach to variations in key hyper parameters (Sec. VI-C), (iv) which parts of the encoder’s input are used to infer the robot’s gait phase (Sec. VI-D), (v) to what extent the locomotion parameters can be varied online (Sec. VI-E), (vi) the feasibility of the locomotion plans produced (Sec. VI-F), (vii) a comparison between the gait parameters seen during training and those shown in experiments using the VAE-planner (Sec. VI-G), (viii) the degree to which disturbance detection, coupled with a rudimentary recovery strategy, further increases the robustness of our approach (Sec. VI-H), and finally, (ix) whether the VAE-planner can be deployed successfully

on the next generation ANYmal C robot without retraining (Sec. VI-I). Please see the following video for an extended set of experiments along with a brief description of our approach (<https://youtu.be/GT2WLh2Ackc>).

### A. Investigating the latent space

We wish to examine if there is any structuring in the latent space as well as investigate if any locomotion properties are disentangled within. This knowledge is crucial in understanding how to solve for locomotion trajectories in latent space.

**Latent Space Structure:** Structure in latent space manifests itself as clustered latent variables. During training, we expect that points in latent space which are of the same gait type will become gathered together. To verify this, we sample a set of random latent variables which we pass through the stance performance predictor. These points are plotted and colour-coded based upon their predicted stance. The resulting plot can be found in Sec. VI-A, specifically in Fig. 5.

**Latent Space Disentanglement:** We wish to see what trajectories in latent space look like, and if any of the dimensions within are interpretable. State-space trajectories of the robot trotting from the test set are encoded into latent-space, and the subsequent latent-space paths are visualised. These paths in latent space are oscillatory and each oscillation has its own phase.

In order to understand what each oscillation encodes, we artificially inject sine waves into each latent dimension in turn. Decoding these trajectories and visualising the joint-space paths reveals that the latent space is indeed disentangled. See Sec. VI-A for full details. This revelation informs how we solve for locomotion paths in latent space.

### B. Backpropagating the binary cross-entropy through the encoder

As in *First Steps* [11], we encourage the latent space to become structured by backpropagating the BCE loss for the contact state of the feet through the encoder. We train an alternative VAE where we detach the BCE gradients at the latent space. This means that the latent-space structure is not informed by the prediction loss of the feet in contact performance predictor. The resulting latent-space of the VAE with detached gradients is compared to the original. Firstly, we look for the crispness of the decision boundaries between stance clusters. Secondly, we look to see if the decision boundaries are aligned with any dimensions in latent space. This analysis is aimed to investigate the importance of using the contact performance predictor to generate feasible locomotion.

### C. Analysing the encoder’s receptive field

In our experiments on the real robot, the VAE is able to infer the robot’s gait phase from raw sensor inputs. We wish to understand which parts of the encoder’s input are utilised to infer this. We utilise activation maximisation (AM) [29] to measure the flow of gradients through the encoder. This procedure requires backpropagating from some randomly sampled input encoding until the encoder output matches a predetermined

target value. The target is chosen to match key points along the robot’s gait phase and are chosen such that the drive signal’s phase is equal to  $0.0, \pi/2, \pi/4, \pi/8, \pi$ . The gradients at the encoder input resulting from this optimisation are recorded. The magnitude of these values reveal which parts of the input are required to infer the gait phase.

#### D. Studying the VAE’s sensitivity to key hyper-parameters

The VAE’s architecture is ablated and the VAE-planner is tested in simulation until the gait phase can no longer be inferred. This leads to noisy and jerky trajectories in simulation. Firstly, the size of the latent dimension is reduced from 125 to a minimum of 6 in strides of 32 units. Secondly, the number of input states  $N$  is reduced from 80 units to 60, sampled at 200 Hz, meaning that the encoded input history reduces from 0.4 s to 0.3 s. Thirdly, the encoder frequency is halved to 100 Hz with  $N = 80$ . Lastly, the widths of the encoder, decoder and performance predictor are reduced in increments of 32 units from 256 to a minimum of 64.

#### E. Varying the gait parameters online

We wish to vary the robot’s gait parameters continuously whilst the robot is walking. This is straight-forward for the robot to do. We utilise a simple ROS publisher with which sets the drive signal’s amplitude, time-period, and stance duration. The robot’s base twist is commanded independently using the action  $a_k$ . In fact, we utilise a navigation waypoint following controller which produces the action so that the robot walks around a square trajectory in our lab.

#### F. Analysing the dynamic feasibility of the VAE’s trajectories

The previous guiding question asks how broad the set of manoeuvres from the VAE-planner are. We now compare the dynamic feasibility of these trajectories to plans from DG. Please note that this dynamic feasibility comparison is undertaken as a post-experiment analysis. On the robot, the output of the VAE-planner is sent directly to the WBC unaltered.

To evaluate the dynamic feasibility of trajectories synthesised by our VAE, we measure the distance of the Zero Moment Point (ZMP) [9] to the support line (i.e. when one pair of legs are swinging) and then compare this distance with that in the synthetic dataset. The ZMP is a commonly used criterion in model-based legged robot control [1], [9]. This analysis is performed for the trajectories in the dataset as a baseline to which we can compare. Dynamically stable trajectories have the ZMP as close as possible to the support line.

#### G. Measuring the distribution of gait parameters achievable with the VAE

The gait parameters set during the robot experiments are recorded meaning that we can measure the distribution of visited states. To show the entire range of movements and compare against those seen during training, we plot a box and whisker plot of the stance and swing durations. This shows the ability of the VAE-planner to generalise producing gait parameters not seen in the training distribution.

#### H. Detecting and reacting to disturbances

We wish to analyse the degree to which disturbances can be detected and whether increasing the robot’s cadence helps the robot to recover from them. As mentioned, we monitor the ELBO as this is a measure of the evidence for an encoded input relative to the learned distribution. Hence, a large spike in this value (given the formulation in Eq. 4) is a consequence of a disturbance.

To perturb the robot, we utilise a push broom and disturb the robot’s base. If the ELBO value surpasses a pre-determined constant, we characterise the event as a disturbance. The ELBO value is calibrated such during normal operation, the ELBO remains below this ”disturbance” threshold. This is easily found by walking the robot using the VAE-planner for 2 min, whilst recording the ELBO.

Following disturbance detection, the VAE-planner automatically reduces the drive signal’s time-period to increase the robot’s cadence. This response is inspired by human locomotion in response to slippage [14]: a group of participants encounter a slippery surface and their reaction is recorded, resulting in an increase in cadence.

We evaluate the effectiveness of increasing the robot’s cadence by repeating the push experiment with and without the cadence increase. The base velocity is utilised to measure the size of the disturbance. Larger velocities arise from bigger pushes. We make a comparison between the reactive VAE-planner and a constant cadence version.

In addition, the latent-space trajectory is inspected during and after a disturbance. We are interested in how this is affected by out of distribution occurrences like a shove from a push broom or a kick to the robot’s base.

#### I. Deployment on ANYmal C without retraining

The VAE which is trained using simulated ANYmal B locomotion data is deployed on ANYmal C without retraining. Since our generative model has successfully transferred from simulation to the real robot, a key question is can the VAE-planner work on a different robot with similar kinematics, but significantly different dynamics? Therefore, we deploy the VAE-planner on a different robot which has a few key differences. Firstly, the ANYmal C has around twice the torque limit of ANYmal B, 80 Nm and 40 Nm respectively. Secondly, ANYmal C is significantly heavier than ANYmal B weighing in at 50 kg to B’s 35 kg. Finally, ANYmal C’s actuators have a lower bandwidth due to the additional reduction gearing. The only alterations made to the VAE-planner are firstly the torques are standardised to reflect the difference in peak torque demand, and secondly, the WBC’s internal dynamics’ model is updated to ANYmal C.

As previously discussed, the VAE-planner can be utilised to measure differences between the learned distribution and the encoded one. Therefore, this approach is able to characterise differences between the two robots. Again, we utilise the ELBO for this, and we record this quantity when the VAE-planner is deployed on ANYmal C. The ELBO distribution can be separated in the KL divergence and the reconstruction error.

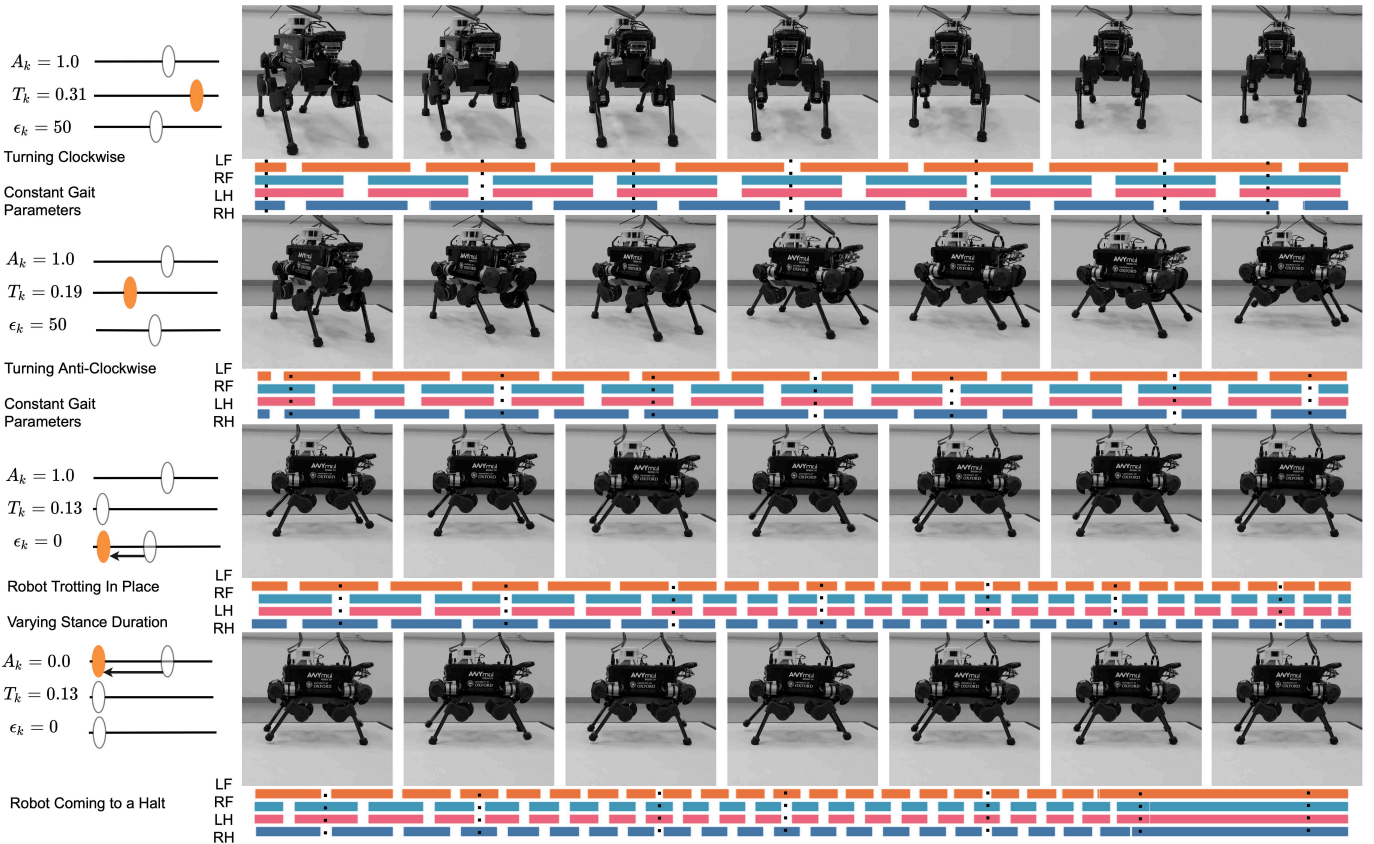


Fig. 4: Closed-loop control of the real ANYmal quadruped using our VAE-planner. This demonstrates user-controlled variation of gait parameters on the fly. Here, coloured rectangles represent the full-stance phase, whilst white space denotes the swing duration. The top row shows a trot gait with an introduced quadrupedal stance phase (gait cycle of 0.75 s – swing 312.5 ms, stance 62.5 ms; a gait cycle consists of a swing phase for each of the leg pairs). Next, the swing duration  $T_k$  is reduced using the time-period slider (gait cycle of 0.5 s – swing 188 ms, stance 62.5 ms). The third row illustrates the effect of reducing the stance duration counter  $\epsilon_k$  to produce trot with reducing full-stance phases (gait cycle of 250 ms – swing 125 ms, stance 0.0 s). Finally, transition into standing occurs when the drive signal amplitude  $A_k$  is reduced to zero. To view the full range of movements, please see the following video <https://youtu.be/GT2WLh2Ack>.

The former provides insight into the distribution of encoded values and the latter acts as a prediction loss.

To verify if the differences in KL-divergence collected from both robots are statistically significant, we utilise a Mann-Whitney U-test [30]. Our null hypothesis is that the median of the distribution from ANYmal B is equal to the median from the distribution from ANYmal C. The values of KL-divergence are collected from deploying the same VAE-planner on both robots. In total, we analyse  $2.5 \times 10^4$  values from each robot, which is equivalent to 62.5 s at 400 Hz. The null-hypothesis is rejected if the resulting p-value is less than our chosen statistical significance value of 0.1%. This procedure is repeated for the two sets of reconstruction error gathered from each robot.

## VI. EXPERIMENTAL RESULTS

Now that we have posed our guiding questions and stated how to answer them, we present the results. These questions can be split up into two categories: (a) introspection of the VAE and (b) analysis of the VAE as a planner deployed on two real-world platforms. Please see the following video for

a complete set of experiments along with a brief description of our approach: <https://youtu.be/GT2WLh2Ack>.

### A. Structure induced in the latent space

The latent space is inspected to discover what structure exists and if any locomotion properties are disentangled within.

**Latent Space Structure:** Fig. 5 shows samples from the latent space colour-coded by their *predicted* stance. For trot, there are four stances: the full-support phase, left front and right hind in contact, another support phase and finally right front plus left hind in contact. Fig. 5 reveals that the latent space has emerged clustered by stance and that, due to the ordering of these stances, a periodic trajectory decodes to a trot gait. This favourable structure is inferred from the continuous trot trajectory input during training.

**Latent Space Disentanglement:** By examining the latent variables, we discover that oscillations injected into just two dimensions in the latent space decode to continuously varying trot trajectories. This result stems from a latent space where variation in footstep length and cadence is aligned along one dimension, while variation in footstep distance lies along



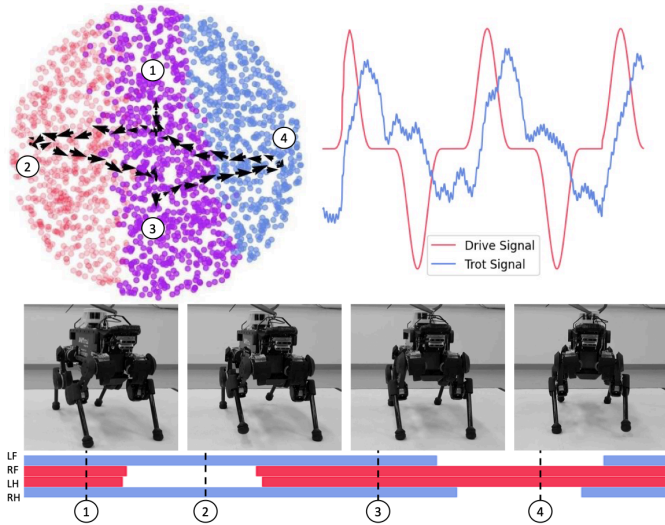


Fig. 5: The latent space and trajectory in black during unperturbed operation. The latent space trajectory is result of the combination of the red drive-signal along the horizontal dimension and the blue trot-signal in the vertical. The drive signal is user controlled, whilst the trot-signal is inferred. The subsequent robot locomotion and contact schedule is included.

another. Specifically, the time period of what we denote the *drive signal* oscillation controls the robot’s cadence, whilst its amplitude is proportionate to the footstep height. In addition, the amplitude of the second signal, which is  $\pi/2$  out of phase with the drive signal, controls foot swing length and as such is denoted as the *trot signal*. Given that other work has tried to explicitly build this structure into locomotion systems [22], it is important to emphasise that this disentanglement *emerges* in our study as a result of the training paradigm and data. Only the synthetic drive-signal needs to be injected into the latent space for closed-loop control; the trot signal is inferred.

**Visualising The Latent-Space Trajectory:** We plot the injected drive-signal and inferred trot signal in Fig. 5 in red and blue respectively. When these two signals are plotted against one another, they combine to form a cycle in latent space. This is plotted as the black-vector field in Fig. 5. This cycle is annotated to show how the latent-space trajectory visits each stance cluster in turn. We also show the corresponding contact schedule with images of the robot in their matching configurations.

To begin at point (1), the robot has four feet in contact, before moving anti-clockwise tracing out a triangular lobe in the red region to point (2). This lobe forms the first foot-swing. The trajectory continues anti-clockwise through the magenta region (3) before tracing another lobe through the blue area back to point (1). This cycle repeats as the robot takes more steps.

### B. Backpropagating the BCE loss through the encoder

We compare the latent space created by backpropagating the BCE gradients through the encoder to the vanilla case, where these gradients are detached before the latent space in Fig. 6. The latent space structured using the BCE gradients

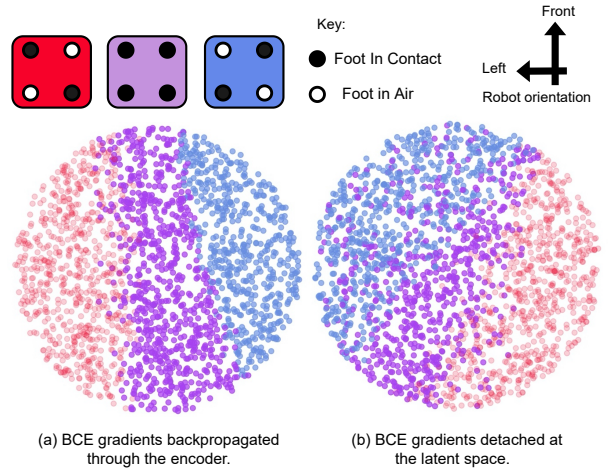


Fig. 6: A comparison of a latent space actively structured using BCE gradients which flow through the encoder’s input (sub-figure (a)) to the vanilla case, where BCE gradients are detached at the latent space (sub-figure (b)). Points in latent space are coloured by their stance. In the key above the latent-space images, a filled-in circle represents a closed contact and a circular outline denotes an open contact.

exhibits crisp decision boundaries for the stance clustering. These boundaries are aligned perpendicular to the drive-signal dimension in latent space, meaning that stance classification results mostly from this dimension. In contrast, the detached gradient latent-space has fuzzy decision boundaries. This is less than ideal as the predicted contact state is an input to the controller, and vitally affects the propagation of the dynamics model. If this is a noisy prediction, the robot will change contact state in an unpredictable way. Note that the decision boundaries in the detached case are rotated at roughly  $30^\circ$  in comparison the nominal case. This results in the latent space being no longer axis aligned with the drive signal. In order to create locomotion trajectories and have independent control over the gait parameters, namely step height and length, the drive signal needs to be rotated to align with the decision boundaries. This is not required for the nominal case, where the BCE gradients are backpropagated through the encoder. Therefore, the crisp decision boundaries and the axis-alignment justifies our decision – and more crucially highlights the importance – of using the BCE gradients to structure the latent space.

### C. Sensitivity To Hyper Parameters

As mentioned in Sec. IV-C, real-time performance is only achievable if VAE inference can be performed in under a 1 ms. Therefore, we report the results of our ablation study where the VAE’s channel capacity is systematically reduced. Table I summarises the results of this study. Firstly, the latent dimension is reduced from 125 to a minimum of 6. The VAE with latent size of 6 units is deployed successfully in simulation and on the real robot. Next, the VAE’s width is reduced in 32-unit increments and a limit of 128 units is found. This corresponds to a reduction in channel capacity by 52.8%.

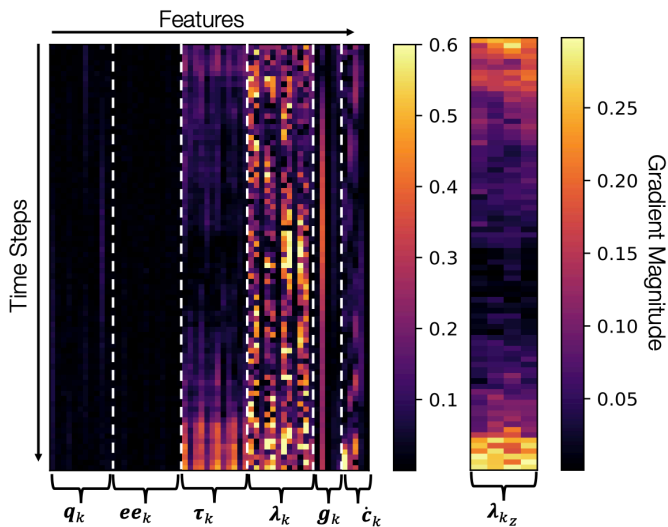


Fig. 7: Visualisation of the encoder’s receptive field with respect to the gait phase. The encoder input is reshaped such that robot state quantities such as joint torques are in the same column. We also show the contact forces normal to the ground plane  $\lambda_{zk}$ . The lightest areas in these two sub-figures are of highest gradient meaning that the encoder focuses on these parts in order to infer the gait phase.

Additionally, the window of time used to construct the VAE’s input is reduced from 0.4 s to 0.3 s whilst maintaining an encoder frequency of 200 Hz. This results in poor open-loop performance as the VAE is no longer able to learn the gait phase. This is a result of the swing duration in the dataset which is 0.45 s. Therefore, an input history over the last 0.3 s is insufficient to capture the gait phase. Next, we investigated reducing the encoder’s sampling frequency  $f_{enc}$  by halving it to 100 Hz whilst the history remains sampled over 0.4 s. Though this speeds up inference, the resulting trajectories are less smooth than the 200 Hz encoder and the robot is not stable during closed-loop operation.

As a result of these analyses, the minimum VAE architecture requires a latent space of 6 units, an input history of 0.4 s sampled at 200 Hz, and a hidden layer size of 128 neurons. We confirm this by deploying this reduced model on the real robot.

TABLE I: We perform an ablation study to find the minimum channel capacity required for the VAE-planner to transfer successfully to the real robot. The original VAE model denoted as (O) is found in the bottom right-hand corner of this table. The latent-space size is reduced to six whilst the width remains 256. The width is reduced to 64 in units of 32. The smallest model which transfers to the real robot has width of 128 and latent size of six.

Latent Size	Model Width				
	64	96	128	192	256
6	F	F	T	T	T
29	-	-	-	-	T
61	-	-	-	-	T
125	-	-	-	-	O

#### D. Analysing the encoder’s receptive field

It is crucial that the VAE is able to infer the robot’s gait phase from raw sensor input to permit successful latent-space planning. This poses the question which parts of the encoder input are used to infer this.

Fig. 7 depicts a saliency map where a brighter colour denotes areas of high gradient. These are areas where the VAE’s encoder focuses in order to infer the gait phase. The left map in Fig. 7 shows the receptive field of the encoder over the entire input  $X_k$ . Here, the input  $X_k$  is reshaped such that each row is the robot state  $x_k$ , see Eq. 1. The columns represent specific robot quantities which we have highlighted in Fig. 7. The areas of high gradient are the contact forces and the most recent joint-torques. The left part of Fig. 7 are the contact forces normal to the ground plane (i.e. the z-direction). This plot reveals that the most recent and earliest contact forces are utilised to infer the gait phase. High values of contact force correlate well with the contact state. Additionally, the joint torques are related to the contact forces through the robot dynamics’ equation [31]. Lastly, the base-velocity has a high gradient value. This quantity is utilised in inferring the robot’s momentum.

#### E. Varying locomotion parameters online

We leverage the disentangled latent-space to smoothly transition between gait parameters whilst the robot is walking. Crucially, cadence, stance duration, and footstep height can be varied during any phase of the gait by modulating the drive signal’s parameters (see Sec. III-A). This results in operating modes which vary from those seen during training. Examples of walking motion using the VAE-planner on the real robot are shown in Fig. 4.

**Swing Duration:** The swing duration is varied over a large operating window on the ANYmal robot. This begins with a swing time-period starting at 312.5 ms, and is smoothly varied until the swing duration reaches 125 ms, effecting a faster step rate. In parallel, we alter the robot’s heading, demonstrating the independence of the action and the latent-space dynamics. Specifically, the top row of Fig. 4 shows the nominal swing duration of 312.5 ms as the robot turns clockwise, tracking a constant angular velocity command. Following this, we demand a slightly faster swing 188 ms and a constant angular velocity anti-clockwise, before transitioning to the fastest swing (125 ms) in the third row. Here, the coloured contact schedule captures the changes in swing duration as it occurs in real-time.

**Stance Duration:** Following a successful reduction in cadence, the stance duration is reduced and the robot transitions into a trot with negligible full-stance phase:  $\epsilon_k = 0$ . Trot gaits with little to no full-support phase are particularly challenging manoeuvres for the system in general, as there is reduced control authority to correct for accrued base pose error. During the swing phase of this gait style, only feet across the diagonal are in contact resulting in a line contact limiting the robot’s ability to steady its base. The transition to a negligible full-stance phase is captured in the third row, where the coloured stance duration reduces in length.

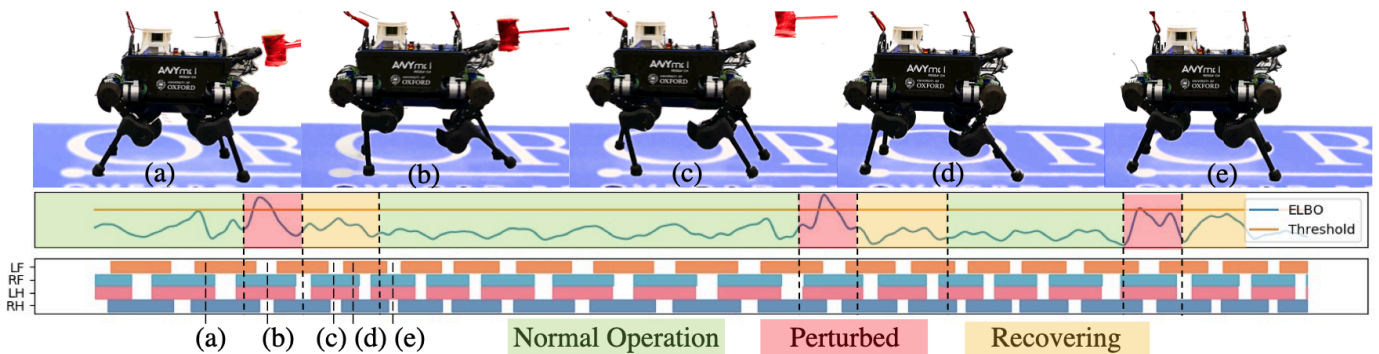


Fig. 8: Push recovery following a shove to the base. A disturbance to the robot causes the ELBO of the form in Eq. 4 to rise above a predetermined threshold (red areas). This identifies a disturbance and triggers an increase in cadence from 250 ms to 125 ms as a rudimentary response. This reduction in the swing duration is visible in the contact schedule. To appreciate the results fully, please see the following video <https://youtu.be/GT2WLh2Ackc>.

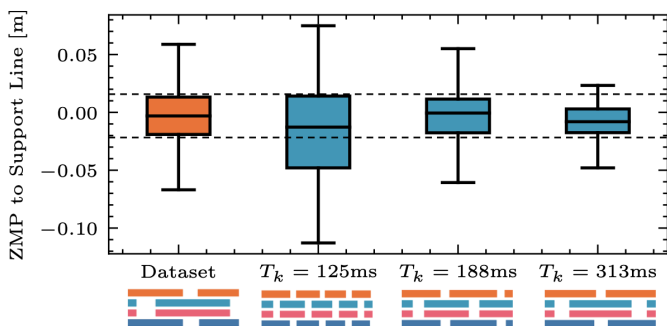


Fig. 9: Distribution of the signed distance between the ZMP and the support line during the 2-stance phases (i.e., one pair of legs was in swing). In orange, the distribution with upper and lower bounds (dashed lines) from the dataset which uses a swing duration of  $T_k = 0.5$  s. In blue, the distribution of the VAE trajectories shown over a range of modes deployed on the real robot.

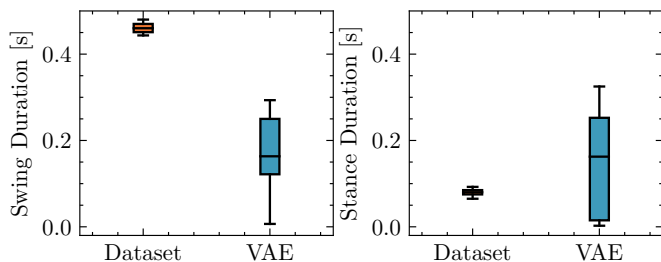


Fig. 10: Comparison of the distributions of swing and full-stance durations between the dataset used for training and the motions executed on the real robot with the VAE and different drive signal parameters during the test presented in Sec. VI-E.

**Footstep Height:** We vary the amplitude of the drive signal smoothly to zero as is seen in the bottom row (Fig. 4): The footstep height reduces to zero as the white-space in the contact schedule disappears and the robot remains standing. Beyond versatility, e.g. to increase swing heights to overcome irregular ground height, this capability further enables a safe, smooth and natural transition into and out of the VAE control mode (i.e. to start and come to a halt).

#### F. Evaluating the dynamic feasibility of planned motions

On the robot, the trajectories from the VAE-planner are sent directly to the WBC unaltered. Here, we compare dynamic feasibility of the trajectories shown in Sec. VI-E after the experiment in order to compare to the training dataset’s distribution generated using DG. The position of the ZMP relative to the support line is utilised as a metric for this comparison. The optimal trajectory will have the ZMP lie on the support line.

The results of this are summarised in Fig. 9. The distribution the ZMP positions is similar for both DG (dataset) and a range of the VAE-planner’s operating modes. Crucially, this remains true despite the maximum swing duration generated by the VAE-planner being up to 3.2 times faster than in the training data. We conclude that the representation is good enough to generalise to the robot’s dynamics shown here. Empirically, we have further been able to steer the robot with arbitrary and fast changing input actions for x, y, and yaw rates, issued from a remote control while being able to interpolate the gait style.

#### G. Generalisation to different gait styles

The VAE is able to produce a far broader range of different trot styles than those in the dataset. The ranges of swing and stance durations produced by the VAE in Sec. VI-E and those in the dataset are summarised in Fig. 10. As discussed previously, the dataset is constructed utilising a pre-determined and constant swing duration of 500 ms, with stance duration of 75 ms. The VAE-planner’s swing duration varies between 312.5 ms and 125 ms and its stance ranges between 325 ms to negligible duration. This demonstrates that the VAE-planner is able to generalise to a variety of trot styles by navigating the structure within the disentangled latent-space, even when trained using a very restrictive training set.

#### H. Disturbance detection and recovery

The robot’s base is pushed using a push broom, and the VAE-planner detects this disturbance by monitoring the ELBO. If the ELBO spikes above a certain threshold, the VAE-planner automatically increases the robot’s cadence as a

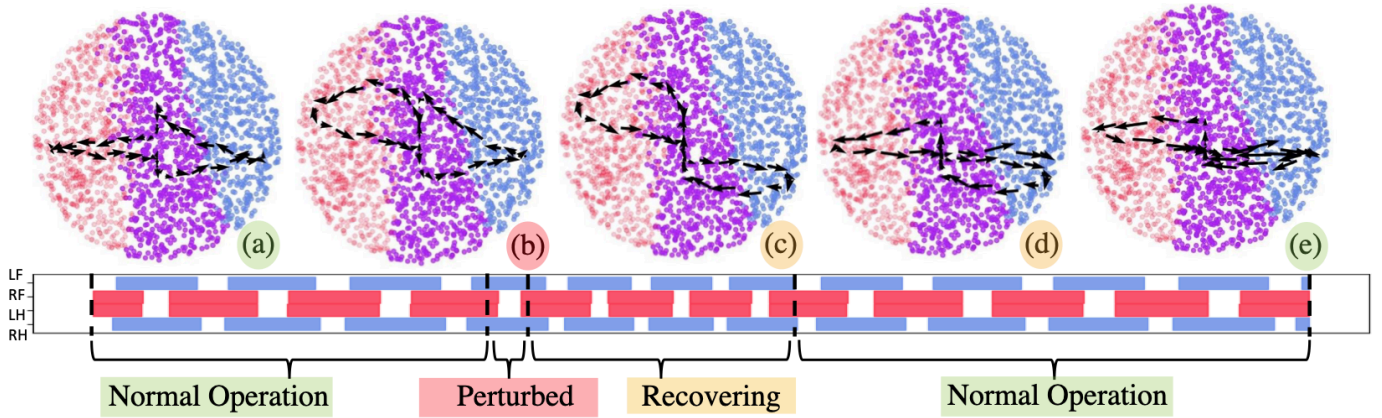


Fig. 11: We show the latent-space trajectory in a series of sub-figures as the robot is walking normally, is perturbed, and recovers. The latent-space trajectory (in black) is plotted on the latent-space colour-coded to show the stances of the trot-gait. In normal operation (sub figures (a) and (e)) the latent-space path is a figure of eight with triangular lobes during the robot’s footswing (blue and red areas). As the robot is perturbed (sub figure (b)), the lobes are far more elongated. Crucially, this elongated trajectory reverts back to the nominal trajectory as the robot recovers. The accompanying footstep schedule is plotted along side.

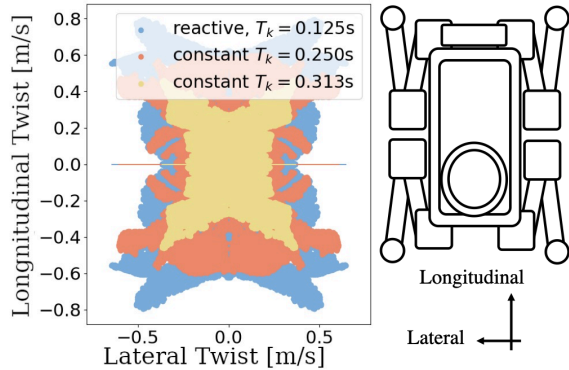


Fig. 12: The range of rejectable base-velocity disturbances increases when automatically modulating the cadence. This plot is symmetrical for ease of view. The range of swing durations plotted is 313 ms, 250 ms, and 125 ms.

rudimentary response. For our push experiments, we choose the ELBO threshold value to be 11.0. We find this value by walking the robot around the lab using the VAE-planner and choosing a value above what is seen during normal operation.

The VAE-planner is able to reject a wide range of impulses applied to the robot’s base. However, this operating window is enlarged by increasing the robot’s cadence as soon as a disturbance is detected. This *reactive* VAE-planner halves the robot’s cadence from a nominal 250 ms to 125 ms once the ELBO threshold is surpassed.

We show the VAE-planner detecting and reacting to the push broom disturbance in Fig. 8. The top row shows the robot being pushed violently before recovering in three to four steps. At point (b) the ELBO spikes above the threshold indicating the disturbance. Throughout the next 1.5 s, the cadence is halved. This is visible in the contact schedule—the white space reduces in width, see point (c). At points (d) and (e) the robot has fully recovered. The ELBO and contact schedule plots continue on and the robot is pushed twice more in this figure.

A comparison between the reactive VAE-planner and a constant cadence version is drawn in Fig. 12. The constant cadence VAE-planner uses swing durations of 313 ms and 250 ms, whilst the reactive version halves the robot’s cadence to 125 ms as described. Here, we see that the range of rejectable push disturbances increases as the swing duration decreases.

Finally, we illustrate what happens to the latent-space trajectory during and after the disturbance. The nominal latent-space trajectory forms a figure of eight and is typified by triangular lobes. This is visible in Fig. 11 sub-figures (a) and (e). When the robot is perturbed these lobes deform and elongate e.g. in sub-figures (b) and (c). The latent-space trajectory converges back to nominal causing the robot to recover as in sub-figures (c) and (d). Finally, the robot has fully recovered and the latent-space trajectory return to nominal (sub-figure (e)).

### I. Transfer to ANYmal C

We successfully deploy the VAE-planner trained using simulated ANYmal B data on ANYmal C. Please note that the VAE is not retrained. The differences between the two robots are significant as ANYmal C’s joint torque limits are 80.0 N m instead of 40.0 N m, and ANYmal C’s total mass is 50 kg instead of 35 kg. Also note that the WBC’s internal model for both kinematics and dynamics are updated when the VAE-planner is deployed on ANYmal C. However, the joint trajectory output from the VAE-planner is the input to the WBC meaning that joint trajectories from the VAE-planner are suitable for ANYmal C.

Despite not retraining, the VAE-planner is able to command ANYmal C’s heading and control the robot’s gait parameters. In essence, the experiment in Sec. VI-E is repeated with the same VAE-planner, but deployed on ANYmal C. Fig. 13 shows ANYmal C with the VAE-planner deployed onboard, along with the contact schedule. The latter shows the variation in both swing and stance duration as the robot walks.

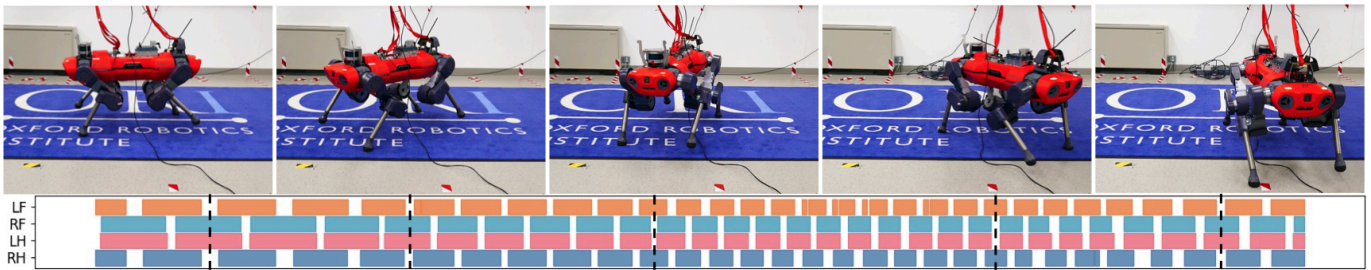


Fig. 13: We deploy our VAE-planner on a different robot: ANYmal C. The VAE used here is trained using data from a simulated ANYmal B robot. ANYmal C is significantly heavier than ANYmal B (50 kg to 35 kg) with twice as much maximum torque, but has actuators with lower bandwidth. With the use of the WBC, the VAE-planner is able to control ANYmal C effectively. The user control over the robot’s base twist using the action and the gait parameters are varied as on ANYmal B using the drive-signal parameters. The variation in gait parameters is captured by the swing and stance durations in the contact schedule below the images of the robot. Please view the ANYmal C locomotion in our video found at <https://youtu.be/GT2WLh2Ack>.

**Comparing ANYmal B and C using ELBO:** The ELBO can be used to further compare the differences between encoding the raw ANYmal B and C data. As mentioned in Sec. V-I, key parameters such as joint torque limits are standardised before encoding. Analysis of the ELBO is split into comparison of the KL divergence and mean-squared reconstruction error between ANYmal B and ANYmal C.

The KL divergence term is particularly affected by latency in the input. For example, if the states in the encoder input are not sampled exactly at the encoder frequency, the KL divergence term will increase. The distributions of these values are quite different between each robot. The KL-divergence values for ANYmal B show a steady mean drift upwards which is negligible for ANYmal C. The median value for ANYmal C is also noticeably lower than for ANYmal B.

As described in Sec. V-I, we compare the KL-divergence values from both robots together using a Mann-Whitney U-test [30]. As a reminder, we record the KL-divergence for both robots and analyse sets of size  $2.5 \times 10^4$ . The resulting U-statistic is  $1.82 \times 10^9$  and the p-value is  $p < 0.001$ . Therefore, the null-hypothesis is rejected and the difference in the median values of the KL-divergence from both robots is statistically significant.

The reason for ANYmal C’s lower median value is down to the relative performance of the onboard computers on the two ANYmals. ANYmal C has a much faster CPU meaning that the VAE-planner’s control loop is comfortably under the 2.5 ms required for real-time control. The result of which is the encoder’s input is sampled at the desired encoder frequency. In contrast, on average the control loop on ANYmal B violates the real-time control law roughly 20% of the time during the experiment run in Fig. 10. This introduces latency into the control loop which causes the increase in KL-divergence.

The reconstruction error for ANYmal B is, unsurprisingly, lower than for ANYmal C. The median value for ANYmal B reconstruction error is  $5.74 \times 10^{-3}$ , whilst for ANYmal C it is  $1.58 \times 10^{-2}$ . These median values are compared using the Mann-Whitney U-test conducted over two sets containing  $2.5 \times 10^4$  values. The U-statistic is  $8.26 \times 10^7$  resulting in a p-value of  $p < 0.001$ . The results in the rejection of the null-hypothesis, meaning that the two distributions are statistically

different. Since the VAE-planner is trained using data from the ANYmal B, a lower reconstruction error is expected.

## VII. CONCLUSION

In this paper, we present a robust and flexible approach for locomotion planning from the perspective of traversing a structured latent-space. This is achieved utilising a deep generative model to capture relevant structure from locomotion data and enables the detection and mitigation of disturbances. The latent space is disentangled to a degree that key salient locomotion features are automatically discovered from a single style of trot gait. An investigation of this latent space reveals a two-dimensional representation which encapsulates the underlying dynamics of the system. This disentanglement is exploited using a drive signal with which dynamically consistent locomotion is generated. Crucially, the amplitude and phase of the drive signal directly control the gait characteristics, namely the cadence, swing height, and full-support duration. Once deployed, the ease with which modulation of the drive signal gives rise to seamless interpolation between gait parameters is demonstrated. Despite generalising to remarkably distinct trot styles compared to the training distribution, the entire range of VAE trajectories remains dynamically consistent. Additionally, utilising a generative model affords the ability to characterise disturbances as out of the distribution seen during training. Though the VAE-planner is able to reject a broad range of impulses applied to the robot’s base, this window is broadened by increasing the cadence as soon as the disturbance is detected. Finally, we show that the approach readily transfers to a kinematically similar but dynamically different platform without needing to be retrained. This helps to showcase the VAE’s ability transfer to new unseen domains.

## ACKNOWLEDGEMENTS

The authors would like to acknowledge the use of the SCAN facility, and thank Oliver Groth for useful discussions.

## REFERENCES

- [1] C. D. Bellicoso, F. Jenelten, C. Gehring, and M. Hutter, “Dynamic locomotion through online nonlinear motion optimization for quadrupedal robots,” *IEEE Robot. Automat. Lett. (RA-L)*, vol. 3, no. 3, pp. 2261–2268, 2018.

- [2] C. Mastalli, W. Merkt, J. Marti-Saumell, H. Ferrolho, J. Solà, N. Mansard, and S. Vijayakumar, “A direct-indirect hybridization approach to control-limited DDP,” *arXiv:2010.00411*, 2021.
- [3] O. Melon, R. Orsolino, D. Surovik, M. Geisert, I. Havoutis, and M. Fallon, “Receding-horizon perceptive trajectory optimization for dynamic legged locomotion with learned initialization,” in *IEEE Int. Conf. Rob. Autom. (ICRA)*, 2021.
- [4] A. W. Winkler, C. D. Bellicoso, M. Hutter, and J. Buchli, “Gait and trajectory optimization for legged systems through phase-based end-effector parameterization,” *IEEE Robot. Automat. Lett. (RA-L)*, vol. 3, no. 3, pp. 1560–1567, July 2018.
- [5] J. Hwangbo, J. Lee, A. Dosovitskiy, D. Bellicoso, V. Tsounis, V. Koltun, and M. Hutter, “Learning agile and dynamic motor skills for legged robots,” *Science Robotics*, vol. 4, no. 26, 2019.
- [6] S. Gangapurwala, A. Mitchell, and I. Havoutis, “Guided constrained policy optimization for dynamic quadrupedal robot locomotion,” *IEEE Robot. Automat. Lett. (RA-L)*, vol. 5, no. 2, pp. 3642–3649, 2020.
- [7] S. Gangapurwala, M. Geisert, R. Orsolino, M. Fallon, and I. Havoutis, “RLOC: Terrain-aware legged locomotion using reinforcement learning and optimal control,” *arXiv preprint arXiv:2012.03094*, 2020.
- [8] A. W. Winkler, F. Farshidian, D. Pardo, M. Neunert, and J. Buchli, “Fast trajectory optimization for legged robots using vertex-based ZMP constraints,” *IEEE Robot. Automat. Lett. (RA-L)*, vol. 2, no. 4, pp. 2201–2208, Oct 2017.
- [9] M. Vukobratovic and B. Borovac, “Zero-moment point - thirty five years of its life,” *Int. J. Hum. Rob. (IJHR)*, vol. 1, pp. 157–173, 2004.
- [10] D. Orin, A. Goswami, and S.-H. Lee, “Centroidal dynamics of a humanoid robot,” *Autonomous Robots*, vol. 35, 10 2013.
- [11] A. L. Mitchell, M. Engelcke, O. Parker Jones, D. Surovik, S. Gangapurwala, O. Melon, I. Havoutis, and I. Posner, “First steps: Latent-space control with semantic constraints for quadruped locomotion,” in *IEEE/RSJ Int. Conf. Intell. Rob. Sys. (IROS)*, 2020, pp. 5343–5350.
- [12] D. Kingma and M. Welling, “Auto-encoding variational bayes,” in *Int. Conf. on Learn. Repr. (ICLR)*, 2014.
- [13] D. J. Rezende, S. Mohamed, and D. Wierstra, “Stochastic backpropagation and approximate inference in deep generative models,” in *Int. Conf. on Mach. Learn. (ICML)*, 2014.
- [14] B. E. Moyer, A. J. Chambers, M. S. Redfern, and R. Cham, “Gait parameters as predictors of slip severity in younger and older adults,” *Ergonomics*, vol. 49, pp. 329–343, 2006.
- [15] A. L. Mitchell, W. Merkt, M. Geisert, S. Gangapurwala, M. Engelcke, O. P. Jones, I. Havoutis, and I. Posner, “Next steps: Learning a disentangled gait representation for versatile quadruped locomotion,” in *IEEE Int. Conf. Rob. Autom. (ICRA)*, 2022.
- [16] M. Karl, M. Soelch, J. Bayer, and P. van der Smagt, “Deep variational bayes filters: Unsupervised learning of state space models from raw data,” in *Int. Conf. on Learn. Repr. (ICLR)*, 2016.
- [17] M. Watter, J. T. Springenberg, J. Boedecker, and M. A. Riedmiller, “Embed to control: A locally linear latent dynamics model for control from raw images,” in *NeurIPS*, 2015.
- [18] M. Y. Seker, M. Imre, J. H. Piater, and E. Ugur, “Conditional neural movement primitives,” in *Rob. Sci. Sys. (RSS)*, 2019.
- [19] A. Srinivas, A. Jabri, P. Abbeel, S. Levine, and C. Finn, “Universal planning networks,” in *Int. Conf. on Mach. Learn. (ICML)*, 2018.
- [20] D. Hafner, T. Lillicrap, I. Fischer, R. Villegas, D. Ha, H. Lee, and J. Davidson, “Learning latent dynamics for planning from pixels,” in *Int. Conf. on Mach. Learn. (ICML)*, vol. 97, 2019, pp. 2555–2565.
- [21] H. Ling, F. Zinno, G. Cheng, and M. Panne, “Character controllers using motion VAEs,” *ACM Trans. Graph.*, vol. 39, 07 2020.
- [22] Y. Yang, T. Zhang, E. Coumans, J. Tan, and B. Boots, “Fast and efficient locomotion via learned gait transitions,” in *Conf. on Rob. Learn. (CoRL)*, 2021.
- [23] I. Higgins, L. Matthey, A. Pal, C. Burgess, X. Glorot, M. Botvinick, S. Mohamed, and A. Lerchner, “ $\beta$ -VAE: Learning basic visual concepts with a constrained variational framework,” in *Int. Conf. on Learn. Repr. (ICLR)*, 2017.
- [24] C. Dario Bellicoso, F. Jenelten, P. Fankhauser, C. Gehring, J. Hwangbo, and M. Hutter, “Dynamic locomotion and whole-body control for quadrupedal robots,” in *IEEE/RSJ Int. Conf. Intell. Rob. Sys. (IROS)*, 2017, pp. 3359–3365.
- [25] J. Hwangbo, J. Lee, and M. Hutter, “Per-contact iteration method for solving contact dynamics,” *IEEE Robot. Automat. Lett. (RA-L)*, vol. 3, no. 2, pp. 895–902, 2018.
- [26] G. A. Pratt and M. M. Williamson, “Series elastic actuators,” in *IEEE/RSJ Int. Conf. Intell. Rob. Sys. (IROS)*, 1995.
- [27] D.-A. Clevert, T. Unterthiner, and S. Hochreiter, “Fast and accurate deep network learning by exponential linear units (elus),” in *Int. Conf. on Learn. Repr. (ICLR)*, 2016.
- [28] M. Hutter, C. Gehring, D. Jud, A. Lauber, C. D. Bellicoso, V. Tsounis, J. Hwangbo, K. Bodie, P. Fankhauser, M. Bloesch, R. Diethelm, S. Bachmann, A. Melzer, and M. Hoepflinger, “ANYmal - a highly mobile and dynamic quadrupedal robot,” in *IEEE/RSJ Int. Conf. Intell. Rob. Sys. (IROS)*, 2016.
- [29] D. Erhan, Y. Bengio, A. Courville, and P. Vincent, “Visualizing Higher-Layer Features of a Deep Network,” University of Montreal, Tech. Rep. 1341, Jun. 2009, also presented at the ICML 2009 Workshop on Learning Feature Hierarchies, Montréal, Canada.
- [30] H. B. Mann and D. R. Whitney, “On a Test of Whether one of Two Random Variables is Stochastically Larger than the Other,” *Ann. Math. Statist.*, vol. 18, no. 1, pp. 50–60, 03 1947.
- [31] M. Mistry, J. Buchli, and S. Schaal, “Inverse dynamics control of floating base systems using orthogonal decomposition,” in *IEEE Int. Conf. Rob. Autom. (ICRA)*, 2010.



**Alexander L. Mitchell** received his M.Eng. from the University of Oxford in 2018. Subsequently, he enrolled at the University of Oxford as a Doctoral candidate. He is currently co-supervised by Professor Ingmar Posner and Dr Ioannis Havoutis at the Oxford Robotics Institute. Alexander’s research interests include optimal control and learning-based methods for path planning and control of legged robots.



**Wolfgang Merkt** received the B.Eng.(Hns) degree in mechanical engineering with management and the M.Sc.(R) and Ph.D. degrees in robotics and autonomous systems from the University of Edinburgh, Edinburgh, U.K., in 2014, 2015 and 2019, respectively.

He is currently a Postdoctoral Researcher at the Oxford Robotics Institute, University of Oxford with I. Havoutis. During his Ph.D., he worked on trajectory optimization and warm starting optimal control for high-dimensional systems and humanoid robots under the supervision of S. Vijayakumar. His research interests include fast learning- and optimization-based methods for planning and control, locomanipulation, and legged robots.



**Mathieu Geisert** received his M. Eng. in Aerospace from Institut Supérieur de l’Aéronautique et de l’Espace SUPAERO (Toulouse, France) in 2013. He then joined the humanoid robotics team Gepetto at LAAS-CNRS (Toulouse, France) where he worked for 5 years in different positions and received his PhD in 2018. From 2018 to 2021, he worked on quadruped robots as a post doctoral researcher in the Dynamic Robot Systems (DRS) group (Oxford Robotics Institute - University of Oxford). From 2021, he has been working as a controls research

engineer at Arrival. His research focuses on Control and Learning for Legged Robots Locomotion.



**Siddhant Gangapurwala** completed his Bachelor of Engineering (B.E.) in Electronics from the University of Mumbai in 2016. In 2017, he joined the AIMS program as a doctoral candidate at the University of Oxford. The following year, Siddhant joined the Dynamic Robot Systems (DRS) group of the Oxford Robotics Institute (ORI) to pursue his DPhil degree with focus on machine learning and optimal control based approaches for robotic locomotion over uneven terrain. He continues to work at DRS as a post-doctoral researcher on locomotion, manipulation and loco-manipulation.



**Oivi Parker Jones** received a D.Phil. in natural language processing at the University of Oxford, U.K. From there he went on to do postdoctoral work in language neuroscience, computational modelling, and the development of neuroimaging methods for large datasets at University College London and at the University of Oxford. He is currently a senior postdoc in the Applied AI Lab (A2I) at the Oxford Robotics Institute, honorary fellow in the Nuffield Department of Clinical Neurosciences, and Hugh Price Fellow in Computer Science at Jesus

College, University of Oxford.



**Ioannis Havoutis** received the M.Sc. in artificial intelligence and Ph.D. in Informatics degrees from the University of Edinburgh, Edinburgh, U.K.

He is a Lecturer in Robotics at the University of Oxford. He is part of the Oxford Robotics Institute and a co-lead of the Dynamic Robot Systems group. His focus is on approaches for dynamic whole-body motion planning and control for legged robots in challenging domains. From 2015 to 2017, he was a postdoc at the Robot Learning and Interaction Group, at the Idiap Research Institute. Previously,

from 2011 to 2015, he was a senior postdoc at the Dynamic Legged System lab the Istituto Italiano di Tecnologia. He holds a Ph.D. and M.Sc. from the University of Edinburgh.



**Martin Engelcke** received the M.Eng. and D.Phil. (Ph.D.) from the University of Oxford, Oxford, UK. He conducted his doctoral and subsequent postdoctoral research between 2015 and 2021 at the Oxford Robotics Institute under the supervision of Prof. Ingmar Posner. He is now a research scientist at DeepMind. His research interests include generative models, representation learning, and reinforcement learning.



**Ingmar Posner** is Professor of Engineering Science at Oxford University, where he leads the Applied Artificial Intelligence Lab. His research aims to enable machines to robustly act and interact in the real world - for, with, and alongside humans. Ingmar's track record in machine perception and decision-making includes seminal work on large-scale learning from demonstration, representation learning for scene understanding and prediction as well as 3D object detection and machine introspection. Currently his research interests revolve around

the use of structured latent spaces for robot perception, planning and control.

Ingmar received an M.Eng. degree in Electronic Systems Engineering from Aston University, Birmingham, U.K., and a D.Phil. degree in bioacoustics from the University of Oxford. He is a founding Director of the Oxford Robotics Institute and, in 2014, co-founded Oxbotica, multi-award winning provider of mobile autonomy software solutions.